# Spin/valley coupled dynamics of electrons and holes at the $MoS_2$-$MoSe_2$ interface

Abhijeet Kumar[1], Denis Yagodkin[1], Nele Stetzuhn[1], Sviatoslav Kovalchuk[1], Alexey Melnikov[2], Peter Elliott[3], Sangeeta Sharma[3], Cornelius Gahl[1], and Kirill I. Bolotin[1,*]

[1]Department of Physics, Freie Universität Berlin, 14195 Berlin, Germany
[2]Institute for Physics, Martin Luther University Halle, 06120 Halle, Germany
[3]Max-Born-Institut für Nichtlineare Optik und Kurzzeitspektroskopie, Max-Born Straße 2a, 12489 Berlin, Germany

*kirill.bolotin@fu-berlin.de

**Keywords:** Transition metal dichalcogenides (TMDs), 2-D semiconductor heterostructures, time-resolved Kerr rotation, spin/valley dynamics, opto-spintronics

## Abstract

The coupled spin and valley degrees of freedom in transition metal dichalcogenides (TMDs) are considered a promising platform for information processing. Here, we use a TMD heterostructure $MoS_2$-$MoSe_2$ to study optical pumping of spin/valley polarized carriers across the interface and to elucidate the mechanisms governing their subsequent relaxation. By applying time-resolved Kerr and reflectivity spectroscopies, we find that the photoexcited carriers conserve their spin for both tunneling directions across the interface. Following this, we measure dramatically different spin/valley depolarization rates for electrons and holes, $\sim$30 $ns^{-1}$ and <1 $ns^{-1}$, respectively and show that this difference relates to the disparity in the spin-orbit splitting in conduction and valence bands of TMDs. Our work provides insights into the spin/valley dynamics of photoexcited carriers unaffected by complex excitonic processes and establishes TMD heterostructures as generators of spin currents in spin/valleytronic devices.

## Introduction

In monolayer transition metal dichalcogenides (TMDs), electron-hole pairs can be selectively excited in either of the two inequivalent but energetically degenerate K and K' valleys in momentum space using circularly polarized light. At the same time, strong spin-orbit coupling in TMDs ensures the coupling of the spin and valley degrees of freedom[1,2]. Rich spintronic properties of TMDs have been confirmed in recent experiments exploring light-induced generation[3,4], spatial transport[5–7], and manipulation of spin/valley polarized excitations[8–11]. In quasi-2D monolayer TMDs, the weak screening of the electron-hole interaction causes the formation of tightly bound excitons[12]. The electron-hole interaction also leads to quick dissociation of excitons and valley depolarization[13]. In contrast, spin/valley polarization of free carriers in TMDs is unaffected by electron-hole recombination and exchange interaction. The spin/valley degree of freedom of these free carriers is hence expected to be a robust information carrier compared to the short-lived excitons. While it has been shown that the spin/valley polarization in monolayer TMDs is at least partially transferred from excitons to the resident carriers[14–18], the mechanism of this transfer is not fully understood.

Van der Waals heterostructures composed of two dissimilar TMDs represent the next logical step in complexity towards spintronic applications. For a heterostructure with type-II band alignment, such as $MoS_2$-$MoSe_2$, it is energetically favorable for an electron and a hole to reside in different materials[19]. Optical excitation of a single material in the heterostructure leads to ultrafast charge transfer across the 2D interface within 50 femtoseconds[20]. Such spatial separation of electrons and holes suppresses both ultrafast electron-hole recombination and electron-hole exchange scattering – the problems plaguing spintronic applications of monolayer TMDs. The potential of TMD heterostructures has been demonstrated in recent experiments that showed valley-polarized interlayer excitons with lifetimes in the order of nanoseconds to microseconds[21–24].

Several key questions regarding spin dynamics in TMD heterostructures remain unanswered. First, while spin-preserving transfer of electrons and holes across a TMD heterostructure interface has been reported[22,25], the sub-picosecond dynamics of spin/valley polarization transfer have not been investigated. Second, the spin lifetimes of the tunneled electrons and holes have not been compared in a single TMD heterostructure. This comparison is especially interesting because of the order of magnitude difference in the spin-orbit interaction strength

for conduction and valence bands in TMDs. While these lifetimes have been reported for individual monolayer TMDs[15,16,26], the dynamics in monolayers are likely dominated by poorly understood localized or dark excitons as well as by resident carriers[14–17,27–30]. In contrast, ultrafast separation of photoexcited electrons and holes in a type-II heterostructure allows isolating the contribution of processes dominated by intralayer excitons. Finally, to the best of our knowledge it is not understood if the process of spin polarization transfer onto resident carriers affects TMD heterostructures.

To address these questions, we apply ultrafast two-color transient reflection and Kerr rotation microscopies with sub-200 fs time resolution. By resonantly exciting one layer of the $MoS_2$-$MoSe_2$ heterostructure with circularly polarized light and probing the transient signal in the other layer, we access the ultrafast spin/valley polarization and population dynamics of electrons and holes. We find that the electrons and holes preserve their spin upon transfer across the heterostructure interface. The spin/valley signal in the latter layer has an apparent build-up time of 150−300 fs, significantly slower than the charge transfer time (<40 fs) for both electrons and holes, also reported previously[20,31,32]. In contrast, we observe distinct relaxation dynamics for electrons and holes in the heterostructure: while electron spins in $MoS_2$ depolarize fast, over tens of picoseconds, the spin/valley lifetime of holes in $MoSe_2$ is limited by their population decay. We attribute this to different spin scattering rates for electrons and holes, which, in turn, originate from the different magnitude of spin-orbit splitting between the conduction and valence bands in TMDs.

## Results

### $MoS_2$-$MoSe_2$ heterostructure

The two components of our heterostructure are picked to be similar (Mo-based), with comparable spin-orbit interaction strengths[33] and exciton binding energy[34]. Figure 1a shows spin texture of a Mo-based monolayer TMD. Circularly polarized excitation near resonance with the optical bandgap of the TMD ("A transition") couples to the transition between the lower conduction sub-band and the higher valence sub-band either in K or K' valley, depending on the excitation chirality. As the $MoS_2$-$MoSe_2$ heterostructure exhibits a type II alignment[35], upon resonant excitation of $MoSe_2$ ($MoS_2$), photoexcited holes (electrons) stay inside the original layer, while electrons (holes) can tunnel into lower-energy states of the other material (Fig. 1b). Figure 1c is an optical image of one $MoS_2$-$MoSe_2$ device (fabrication details are in Supporting Information). Low temperature (5 K) photoluminescence (PL) spectra (Fig. 1d) from these monolayer regions exhibit neutral (X) and charged (T) exciton peaks, at 1.65 eV and 1.62 eV for $MoSe_2$ (top panel) and at 1.96 eV and 1.93 eV for $MoS_2$ (middle panel), respectively[36,37]. The intralayer emission from the heterostructure region (bottom panel) are redshifted compared to those of the isolated monolayers, likely due to modified screening[38]. Significantly quenched emission of these peaks suggests efficient charge transfer across the 2D interface[20,39]. In addition, a new peak at 1.42 eV, a tell-tale sign of type-II heterostructures, originates from interlayer exciton (IX) emission and indicates strong interlayer coupling. The spectral features of both monolayers in the heterostructure are well separated and can be pumped and probed selectively.

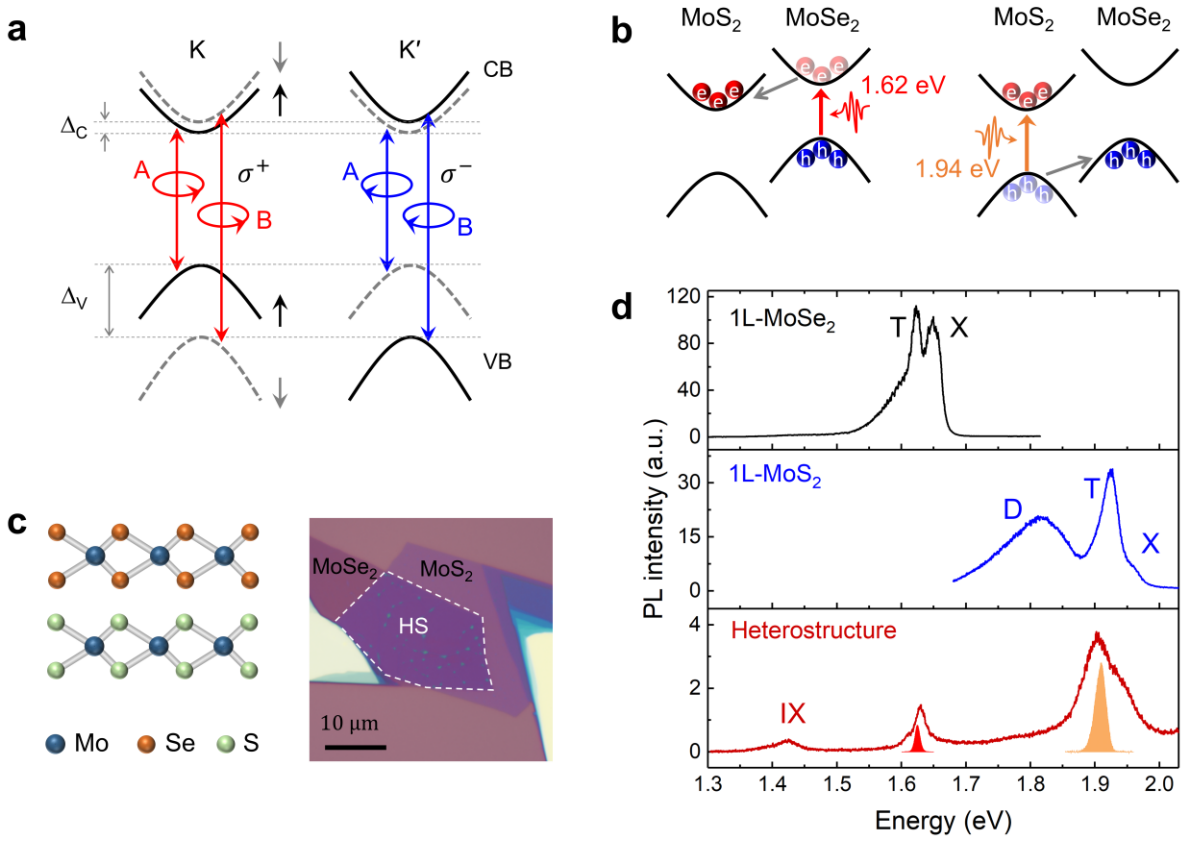


***Figure 1: TMD spin texture and heterostructure characterization.*** ***(a)*** *Spin texture in a Mo-based monolayer TMD. Spin-orbit interaction leads to strong spin-splitting of the valence bands (147 meV for $MoS_2$ and 186 meV for $MoSe_2$) and weak splitting of the conduction bands (3 meV for $MoS_2$ and 21 meV for $MoSe_2$) both at K and K' valleys*[33]*. Coupled spin/valley degree of freedom can be selectively excited using circularly polarized light.* ***(b)*** *The response of a $MoS_2$-$MoSe_2$ heterostructure to photoexcitation. Following light absorption by individual layers, electrons and holes tunnel into energetically favourable states in $MoS_2$ and $MoSe_2$, respectively.* ***(c)*** *Left: cartoon view of the heterostructure. Right: optical image of the assembled device on a $SiO_2$/Si substrate. Dashed white line shows the heterostructure boundary. In addition, the device also contains areas of monolayer $MoS_2$ and monolayer $MoSe_2$.* ***(d)*** *Photoluminescence spectra of monolayer $MoSe_2$ (top panel), monolayer $MoS_2$ (middle panel), and the heterostructure (bottom panel) at 5 K. Monolayer $MoS_2$ also exhibits broad defect-assisted emission (D) at 1.8 eV*[40]*. Significantly quenched emission from the heterostructure along with an interlayer exciton peak (IX) at 1.42 eV suggest efficient charge transfer across the interface. Two shaded peaks in the bottom panel, red at 1.62 eV and orange at 1.91 eV, show the spectra of pump/probe beams tuned to $MoSe_2$ and $MoS_2$ optical bandgap, respectively. The differential reflectivity spectra for this heterostructure are in Supporting Information.*

## Ultrafast spin/valley polarization transfer of electrons and holes

Figure 2a shows the setup for pump-probe Kerr rotation and transient reflectivity measurements (details are in Supporting Information). The photon energies of pump and probe, shown as red and orange shaded regions in Fig. 1d (bottom panel), were tuned to the excitonic resonances of the respective materials. The transient reflectivity signal for probe in resonance with the A transition corresponds to the total pump-induced population change in the relevant

sub-bands at K and K' valleys[41] (Fig. 1a). At the same time, the Kerr rotation angle, $\theta_K$, measures the polarization axis rotation of the reflected probe, and is roughly proportional to the population imbalance between the same sub-bands at K and K' valleys[18]. The population imbalance between K and K' valleys of higher conduction sub-bands or lower valence sub-bands can also be accessed by tuning the probe wavelength to the resonance with the B transition (Fig. 1a).

We first focus on the spin/valley and population dynamics in the $MoS_2$-$MoSe_2$ heterostructure during the first picosecond following photoexcitation in one of the layers. Figure 2b shows the time-resolved Kerr signal under excitation at the $MoSe_2$ optical bandgap ($h\nu_{pump}$ = 1.62 eV) and probe at the $MoS_2$ optical bandgap ($h\nu_{probe}$ = 1.91 eV) for different pump polarization. In this case, excited electrons tunnel from $MoSe_2$ to $MoS_2$. The transient Kerr signal is odd with respect to the pump chirality, $\theta_K(\sigma^+) = -\theta_K(\sigma^-)$, and vanishes for linear pump polarization. To confirm that the transient Kerr signal indeed originates from pump-induced charge transfer across the heterostructure interface, we examine a spatial map of the Kerr signal intensity, $\theta_K(\sigma^+) - \theta_K(\sigma^-)$, at 2 ps delay (Fig. 2c). The signal is uniform across the heterostructure, while no Kerr signal is observed from monolayer regions. We find similar behavior for the case of holes tunneling from $MoS_2$ to $MoSe_2$ (Supporting Information). In Fig. 2d, we compare the time evolution of the reflectivity (gray traces) and Kerr (blue traces) signals in $MoSe_2$ (sensitive to tunneled holes, upper panel in Fig. 2d) and in $MoS_2$ (sensitive to tunneled electrons, lower panel in Fig. 2d), respectively, within the first 1.5 ps after optical excitation. For both excitation schemes, the transient reflectivity signal rises on the timescale of our time resolution. The rise of Kerr signal, in contrast, is delayed and reaches its maximum at a delay of 1–2 ps.

The appearance of Kerr signal for probe resonant with the optical bandgap (Fig. 2b-d) indicates an imbalance between K and K' valleys of the lower conduction sub-bands for electrons and higher valence sub-bands for holes (Fig. 1a). We note that the photoexcited carriers have excess kinetic energy and may relax into higher lying sub-bands[35]. To account for spin contribution from these sub-bands, we observe that the Kerr signal probed at B transition is opposite in sign compared to the previously considered case of probing at the optical bandgap (Supporting Information). Since the Kerr signal probed at B transition is sensitive to the K/K' valley population imbalance of higher conduction sub-bands of $MoS_2$ (Fig. 1a), this indicates that the valley polarization of higher sub-bands is opposite compared to that of lower sub-bands and that their spin polarization is the same. Therefore, we conclude that the spin degree of freedom is conserved during tunneling[22,25], consistent with previous reports of charge transfer being faster than spin/valley depolarization of intralayer excitons[42].

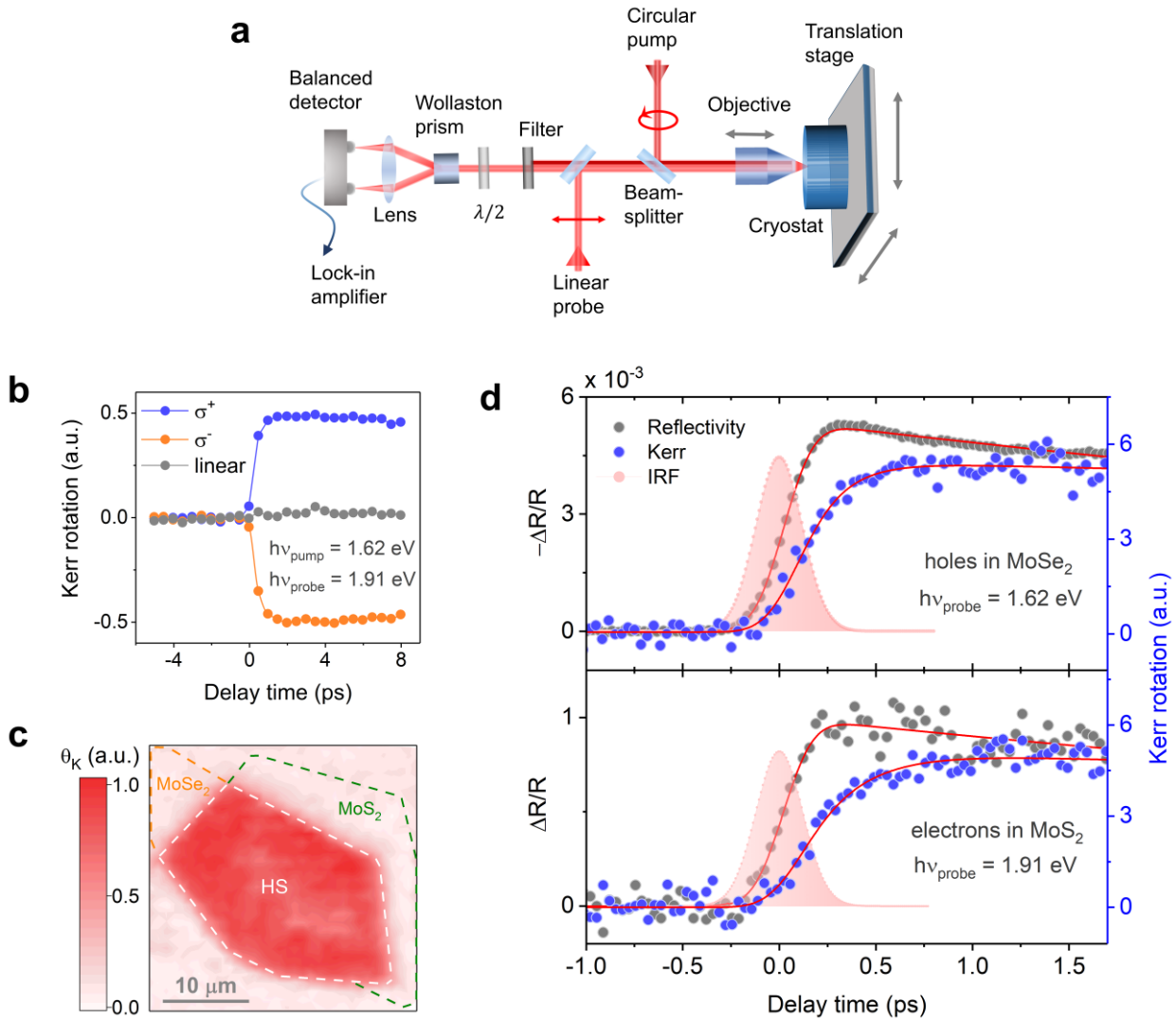


***Figure 2: Charge and spin/valley dynamics in $MoS_2$-$MoSe_2$ on the picosecond timescale.*** ***(a)*** *Time-resolved Kerr/reflectivity setup.* ***(b)*** *Kerr rotation dynamics for the case of pumping $MoSe_2$ and probing $MoS_2$. The odd nature of Kerr signal with pump chirality indicates spin/valley polarization in $MoS_2$.* ***(c)*** *Spatial map of Kerr signal at 2 ps time delay under the same experimental conditions as b). The appearance of Kerr signal only from the heterostructure region confirms that it originates from the transfer of spin-polarized electrons across the heterostructure interface.* ***(d)*** *Evolution of transient reflectivity (gray) and Kerr signal (blue) for holes (upper panel) and electrons (lower panel) together with the cross-correlation of the two laser pulses (IRF, shaded red). To access the case of holes tunneling, pump and probe energies are fixed to 1.94 eV and 1.62 eV, respectively. To extract the rise time, we fit the data (red lines) with the sum of an exponential rise and a slow exponential decay function convolved with the IRF.*

From the fit to the data in Fig. 2d, we estimate the charge transfer time to be less than 40 fs for both electrons and holes, consistent with previous reports[20,31,32]. For the delayed evolution of the Kerr signal, we extract time constants of 250 ± 70 fs for electrons and 170 ± 40 fs for holes (Supporting Information). To understand the apparent delay of the Kerr signal compared to reflectivity, we performed theoretical modelling of time-dependent Kerr spectra (Supporting Information). This modelling confirms that while the reflectivity signal originates at least in

part from phenomena such as screening and bandgap renormalization that are insensitive to the energy of the carriers[43], the Kerr signal is caused by carrier population imbalance close to the extrema of conduction and valence bands at the K/K' valleys[4]. Therefore, we expect a strong reflectivity change but almost no Kerr signal from the hot tunneled carriers immediately following their injection. The carriers are then expected to relax to the band edges on sub-picosecond time scale via strong electron-electron and electron-phonon interactions[44,45] and the Kerr signal should emerge. We therefore suggest that the delayed rise of the Kerr signal reflects cooling dynamics of hot spin-polarized carriers injected across the heterostructure interface.

**Dynamics of electrons and holes after 1 ps**

The decay of photoexcited electron and hole population as well as depolarization of their spin/valley degree of freedom proceeds on timescales >1 ps, longer compared to the timescale of hot carrier cooling. Figure 3 is the central result of our paper comparing the reflectivity (gray trace) and Kerr signals (blue trace) for the cases of pumping $MoS_2$ and probing $MoSe_2$ (accessing tunneled holes, Fig. 3a) and vice versa (accessing tunneled electrons, Fig. 3b). The hole population dynamics (Fig. 3a, gray points) are fitted with a bi-exponential decay with fast $\tau_1^{\mathrm{h,p}} = 30 \pm 2$ ps and slow $\tau_2^{\mathrm{h,p}} = 420 \pm 40$ ps components. For electrons (Fig. 3b, gray points), we observe similar dynamics with components $\tau_1^{\mathrm{e,p}} = 63 \pm 7$ ps and $\tau_2^{\mathrm{e,p}} = 676 \pm 75$ ps. In contrast to the population dynamics, the spin/valley dynamics differ greatly between electrons and holes. For holes, we again observe a bi-exponential decay with fast $\tau_1^{\mathrm{h,s}} = 38 \pm 3$ ps and slow $\tau_2^{\mathrm{h,s}} = 640 \pm 70$ ps components (Fig. 3a, blue points). For electrons, in contrast, we observe a fast mono-exponential decay with a much shorter lifetime $\tau^{\mathrm{e,s}} = 28 \pm 1$ ps (Fig. 3b, blue points).

We speculate that similar lifetimes of electron and hole population in our heterostructure reflect electron/hole recombination across the interface. Interestingly, while we do observe IX emission in our heterostructure (Fig. 1d), much longer lifetimes in the nanosecond range have been measured for these excitons via time-resolved PL measurements[21,22,24]. This suggests that the recombination may be dominated by a defect-assisted nonradiative pathway, also predicted in a recent report[31]. The observation of somewhat different lifetimes for electrons and holes as well as of slow and fast decay components may reflect the variation in the defect densities between the two materials[21]. The confounding effects such as energy transfer, intralayer dynamics, exchange interaction, and photocarrier diffusion that could potentially contribute to the data in Fig. 3 are considered in Supporting Information[22,46–50].

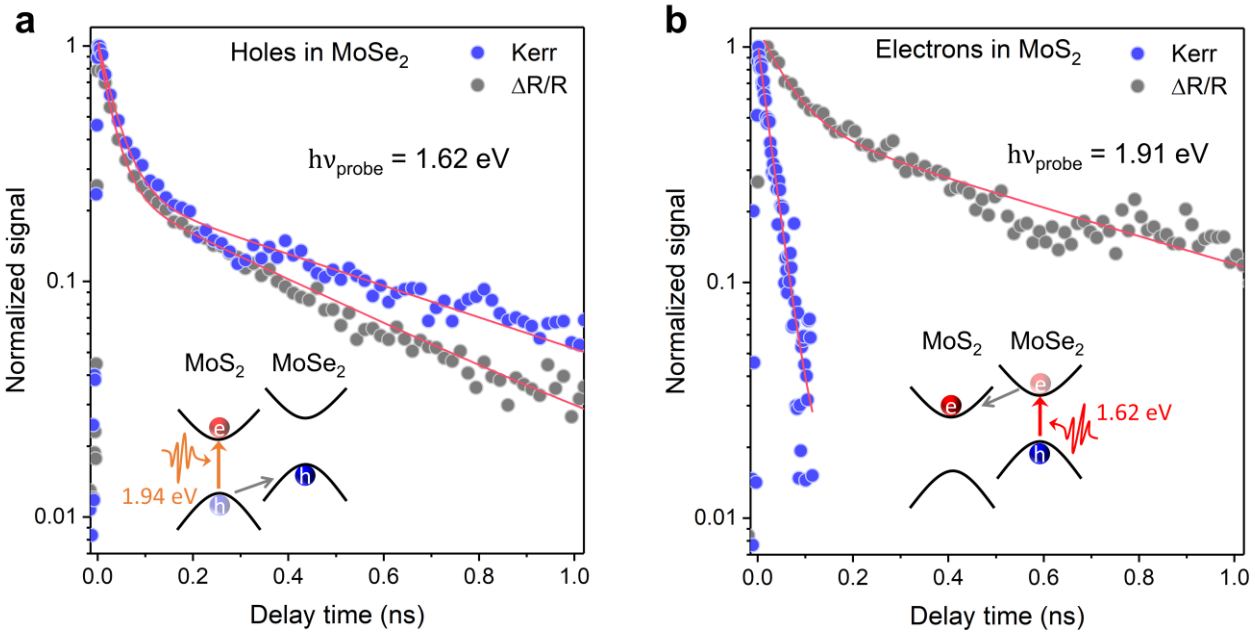


***Figure 3: Charge and spin/valley dynamics of electrons and holes in $MoS_2$-$MoSe_2$ on 1 ns timescale. (a)*** *Time-resolved dynamics for the case of pumping $MoS_2$, probing $MoSe_2$. These traces are interpreted as the dynamics of carrier population (gray) and spin/valley population imbalance (blue) for holes in $MoSe_2$.* ***(b)*** *Corresponding case of pumping $MoSe_2$ and probing electrons in $MoS_2$. Red lines are fits to the data.*

In general, the measured spin/valley lifetime may originate from two different mechanisms. First, it may be limited by the scattering processes leading to spin/valley depolarization. Second, it may simply result from the population decay of excited carriers even in the absence of spin polarization loss. To distinguish between these two mechanisms, we introduce the degree of spin/valley polarization

$$P = \frac{P_+ - P_-}{P_+ + P_-}$$

Here $P_+$ and $P_-$ are the transient population densities in the lowest-energy sub-bands of K and K' valleys, respectively. Experimentally, we can determine $P$ by noting that our transient reflectivity signal is approximately proportional to the total population of excited carriers $(P_+ + P_-)$, while the Kerr signal is proportional to the valley population imbalance $(P_+ - P_-)$. Figure 4 shows $P$ determined from the ratio of Kerr and reflectivity signals. For electrons (Fig. 4, red trace), we observe a mono-exponential decay of $P$ with a decay time of 30 ps, identical to what is seen in Fig. 3b. In contrast, the degree of spin/valley polarization for holes remains almost constant, within uncertainty, over our delay time window of 1 nanosecond (Fig. 4, blue trace). This means that the decay of the Kerr signal for holes in $MoSe_2$ in Fig. 3a is fully caused by the loss of carrier population and the intrinsic rate of hole valley depolarization is significantly lower than 1 $ns^{-1}$.

## Discussion

Summarizing our interpretations so far, the fast Kerr signal decay (<30 ps) observed in $MoS_2$ is determined by the fast spin/valley depolarization of electrons in $MoS_2$, while the much slower Kerr signal decay (>600 ps) measured in $MoSe_2$ is determined by the population lifetime of photoexcited holes. Such trend is seen in all measured samples (Supporting Information), confirming that stacking angle does not significantly influence spin transfer and relaxation dynamics of electrons and holes[25,31]. The difference between spin/valley lifetimes for electrons and holes is noteworthy since most of the material parameters of $MoS_2$ and $MoSe_2$ are similar except for the strength of spin-orbit interaction. A small splitting of ~3 meV in the $MoS_2$ conduction band facilitates rapid intravalley and intervalley scattering of electrons[33]. Spin-flip intravalley scattering may arise due to magnetic impurities or phonon-assisted processes (e.g. via phonons with near zero momentum[51]). Intervalley scattering of electrons may be mediated by longitudinal acoustic (LA) phonons[52–54] leading to rapid spin/valley depolarization. In contrast to electrons, both intra- and intervalley scattering of holes are suppressed due to the spin-splitting of the $MoSe_2$ valence band, ~186 meV, which is much larger than available phonon energies[33] We therefore suggest that the difference between spin/valley depolarization rates for electrons and holes is related to the difference in the strength of spin-orbit interactions in conduction and valence bands of TMDs. This conclusion is further supported by the experiments on other TMD heterostructures reported in Supporting Information.

The arguments above also show that the process of intervalley scattering may effectively render the electrons in $MoS_2$ "invisible" for probing at the optical bandgap by scattering them into the higher conduction sub-bands. To analyze that contribution, we probe the decay of Kerr signal at the energy corresponding to the B transition in $MoS_2$. The measured decay dynamics of this signal are identical to the dynamics probed resonantly with the optical bandgap (Supporting Information). This confirms that the spin-polarization of electrons decays at the same rate in both sub-bands that is likely determined by the efficiency of spin-flip intravalley scattering (Supporting Information). Overall, we conclude that the measured decay dynamics of $P$ (Fig. 4) reflects the decay of spin polarization of all excited electrons and all excited holes, with rates 30 $ns^{-1}$ and <1 $ns^{-1}$, respectively. To the best of our knowledge, this is the first direct comparison of spin lifetime of electrons and holes in a TMD heterostructure.

Strikingly different electron and hole spin lifetimes in our heterostructure are consistent with recent measurements of spin lifetimes in a doped monolayer TMD[15,16]. The nature of the state exhibiting the long spin lifetime in these monolayers is still debated, however. It has been suggested that the spin polarization of relatively short-lived intralayer excitons is transferred onto other long-lived states including resident carriers[14,15,18,43,55], localized states[16,29,30], or dark excitons[27,28]. In contrast, in a type-II heterostructure employed here, electrons and holes are separated between the layers and various states complicating the interpretation of monolayer measurements do not arise. The lack of Kerr signal after the decay of the excited population in our devices (unlike in the measurements of ref.[43,55]) suggests that the process of spin transfer onto resident carriers is not effective. We also note that very long valley lifetimes in the microsecond range were reported for holes in similar heterostructures[41,56]. We speculate that significantly longer lifetimes compared to our measurements may be related to the different measurement scheme of ref.[41,56], where the same TMD layer was excited and probed.

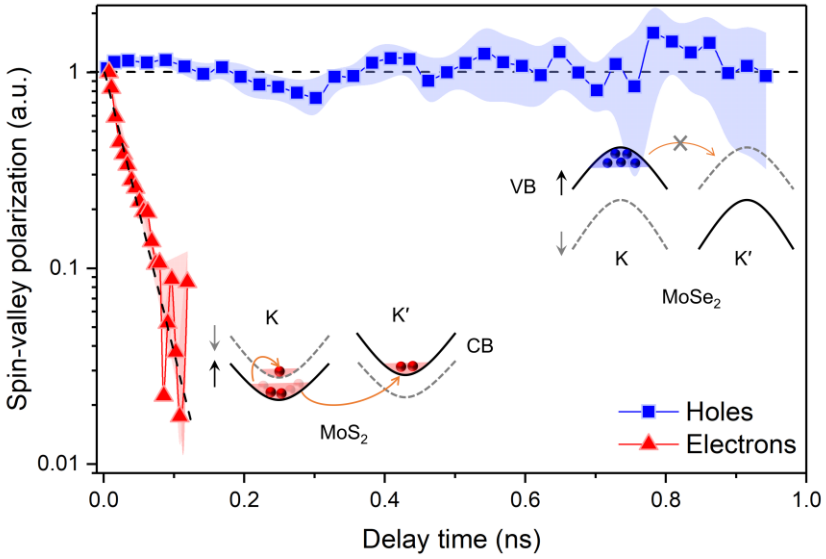


***Figure 4: Spin/valley polarization for electrons and holes.*** *Spin/valley polarization dynamics for electrons in $MoS_2$ (red triangles) and holes in $MoSe_2$ (blue squares). Electrons in the lower conduction sub-band in K/K' valley can undergo rapid intravalley and intervalley scattering, contributing to the equilibration of the valley polarization of the lower sub-bands (inset, bottom). Holes retain their spin/valley polarization over a delay range of 1 ns owing to suppressed intervalley scattering (inset, right). The signal is normalized with respect to the spin/valley polarization at zero delay. Dashed black line is a guide to the eye.*

## Conclusion

We showed, using a combination of transient Kerr and reflectivity microscopies, that the photoexcited electrons and holes cross the $MoS_2$-$MoSe_2$ heterostructure interface within 40 fs while largely preserving their spin. The cooling dynamics of hot tunneled carriers determine the timescale of spin/valley polarization build up. Subsequently, we observe rapid decay of electron spin/valley polarization with a time constant of 30 ps, while the rate of spin/valley depolarization for holes is lower than 1 $ns^{-1}$. The difference in the rates of spin/valley depolarization between electrons and holes is explained by the disparity of spin-orbit splitting between conduction and valence bands in TMDs. To the best of our knowledge, this is the first study reporting the spin/valley lifetimes of electrons and holes in a TMD heterostructure. Our results are relevant for the emerging use of TMD heterostructures as sources of spin/valley polarized currents in layered materials. Finally, we note that it will be interesting to investigate the initial stages of the spin/charge transfer across the TMD interface with techniques capable of resolving sub-100 fs dynamics. It will be equally interesting to analyze the effect of defects, which likely provide the momentum needed for the carriers to cross the TMD interface.

## Author contributions

K.I.B., and C.G. conceived the project; K.I.B., C.G., and A.M. designed the experiment; A.K., D.I., N.S., and S.K. fabricated and characterized the samples; A.K., D.I., and N.S. performed the experiments; A.K. analyzed the data; P.E., and S.S. performed theoretical calculations; A.K., K.I.B., and C.G. wrote the paper with contributions from all other co-authors.

## Notes
The authors declare no competing interests.

## Supporting information
Upper limit of reflectivity and spin/valley polarization rise time;
Evolution of Kerr and reflectivity signal in $MoS_2$;
Analysis of confounding effects;
Methods;
Comparison of spin/valley dynamics between conduction sub-bands in $MoS_2$;
Spin/valley and population dynamics in $MoSe_2$ under non-resonant excitation;
Pump fluence dependence of hole population dynamics;
Comparison of spin/valley dynamics between electrons and holes in $WS_2$-$MoSe_2$ heterostructure;
Differential reflectivity spectra of $MoS_2$-$MoSe_2$ at 6 K;
Band structure in $MoS_2$ and change in density of states upon spin injection;
Simulated absorption and Kerr response in $MoS_2$;
Probe energy dependent Kerr signal rise time;
Spin/valley depolarization of electrons in $MoS_2$ conduction band;
Sample variation of spin/valley dynamics.

## Acknowledgements
We acknowledge the German Research Foundation (DFG) for financial support through the Collaborative Research Center TRR 227 Ultrafast Spin Dynamics and ERC Starting grant no. 639739. We thank Ben Weintrub for technical help.

## References:


(1) Xiao, D.; Liu, G. Bin; Feng, W.; Xu, X.; Yao, W. Coupled Spin and Valley Physics in Monolayers of $MoS_2$ and Other Group-VI Dichalcogenides. *Phys. Rev. Lett.* **2012**, *108* (19), 196802.

(2) Xu, X.; Yao, W.; Xiao, D.; Heinz, T. F. Spin and Pseudospins in Layered Transition Metal Dichalcogenides. *Nat. Phys.* **2014**, *10* (5), 343–350.

(3) Mak, K. F.; He, K.; Shan, J.; Heinz, T. F. Control of Valley Polarization in Monolayer $MoS_2$ by Optical Helicity. *Nat. Nanotechnol.* **2012**, *7* (8), 494–498.

(4) Cao, T.; Wang, G.; Han, W.; Ye, H.; Zhu, C.; Shi, J.; Niu, Q.; Tan, P.; Wang, E.; Liu, B.; Feng, J. Valley-Selective Circular Dichroism of Monolayer Molybdenum Disulphide. *Nat. Commun.* **2012**, *3*, 887.

(5) Mak, K. F.; McGill, K. L.; Park, J.; McEuen, P. L. Valleytronics. The Valley Hall Effect in $MoS_2$ Transistors. *Science.* **2014**, *344* (6191), 1489–1492.

(6) Onga, M.; Zhang, Y.; Ideue, T.; Iwasa, Y. Exciton Hall Effect in Monolayer $MoS_2$. *Nat. Mater.* **2017**, *16* (12), 1193–1197.

(7) Radisavljevic, B.; Radenovic, A.; Brivio, J.; Giacometti, V.; Kis, A. Single-Layer $MoS_2$ Transistors. *Nat. Nanotechnol.* **2011**, *6* (3), 147–150.

(8) Jones, A. M.; Yu, H.; Ghimire, N. J.; Wu, S.; Aivazian, G.; Ross, J. S.; Zhao, B.; Yan, J.; Mandrus, D. G.; Xiao, D.; Yao, W.; Xu, X. Optical Generation of Excitonic Valley Coherence in Monolayer $WSe_2$. *Nat. Nanotechnol.* **2013**, *8* (9), 634–638.

(9) Hao, K.; Moody, G.; Wu, F.; Dass, C. K.; Xu, L.; Chen, C. H.; Sun, L.; Li, M. Y.; Li, L. J.; MacDonald, A. H.; Li, X. Direct Measurement of Exciton Valley Coherence in Monolayer $WSe_2$. *Nat. Phys.* **2016**, *12* (7), 677–682.

(10) Ye, Z.; Sun, D.; Heinz, T. F. Optical Manipulation of Valley Pseudospin. *Nat. Phys.* **2017**, *13* (1), 26–29.

(11) Xie, L.; Cui, X. Manipulating Spin-Polarized Photocurrents in 2D Transition Metal Dichalcogenides. *Proc. Natl. Acad. Sci.* **2016**, *113*, 3746-3750.

(12) He, K.; Kumar, N.; Zhao, L.; Wang, Z.; Mak, K. F.; Zhao, H.; Shan, J. Tightly Bound Excitons in Monolayer $WSe_2$. *Phys. Rev. Lett.* **2014**, *113* (2), 026803.

(13) Yu, T.; Wu, M. W. Valley Depolarization Due to Intervalley and Intravalley Electron-Hole Exchange Interactions in Monolayer $MoS_2$. *Phys. Rev. B - Condens. Matter Mater. Phys.* **2014**, *89* (20), 205303.

(14) Hsu, W. T.; Chen, Y. L.; Chen, C. H.; Liu, P. S.; Hou, T. H.; Li, L. J.; Chang, W. H. Optically Initialized Robust Valley-Polarized Holes in Monolayer $WSe_2$. *Nat. Commun.* **2015**, *6*, 8963.

(15) Dey, P.; Yang, L.; Robert, C.; Wang, G.; Urbaszek, B.; Marie, X.; Crooker, S. A. Gate-Controlled Spin-Valley Locking of Resident Carriers in $WSe_2$ Monolayers. *Phys. Rev. Lett.* **2017**, *119* (13), 137401.

(16) Ersfeld, M.; Volmer, F.; Rathmann, L.; Kotewitz, L.; Heithoff, M.; Lohmann, M.; Yang, B.; Watanabe, K.; Taniguchi, T.; Bartels, L.; Shi, J.; Stampfer, C.; Beschoten, B. Unveiling Valley Lifetimes of Free Charge Carriers in Monolayer $WSe_2$. *Nano Lett.* **2020**, *20* (5), 3147–3154.

(17) Song, X.; Xie, S.; Kang, K.; Park, J.; Sih, V. Long-Lived Hole Spin/Valley Polarization Probed by Kerr Rotation in Monolayer $WSe_2$. *Nano Lett.* **2016**, *16* (8), 5010–5014.

(18) Yang, L.; Sinitsyn, N. A.; Chen, W.; Yuan, J.; Zhang, J.; Lou, J.; Crooker, S. A. Long-Lived Nanosecond Spin Relaxation and Spin Coherence of Electrons in Monolayer $MoS_2$ and

$WS_2$. *Nat. Phys.* **2015**, *11* (10), 830–834.
(19) Ceballos, F.; Bellus, M. Z.; Chiu, H. Y.; Zhao, H. Ultrafast Charge Separation and Indirect Exciton Formation in a $MoS_2$-$MoSe_2$ van Der Waals Heterostructure. *ACS Nano* **2014**, *8* (12), 12717–12724.
(20) Hong, X.; Kim, J.; Shi, S. F.; Zhang, Y.; Jin, C.; Sun, Y.; Tongay, S.; Wu, J.; Zhang, Y.; Wang, F. Ultrafast Charge Transfer in Atomically Thin $MoS_2$/$WS_2$ Heterostructures. *Nat. Nanotechnol.* **2014**, *9* (9), 682–686.
(21) Nagler, P.; Plechinger, G.; Ballottin, M. V.; Mitioglu, A.; Meier, S.; Paradiso, N.; Strunk, C.; Chernikov, A.; Christianen, P. C. M.; Schüller, C.; Korn, T. Interlayer Exciton Dynamics in a Dichalcogenide Monolayer Heterostructure. *2D Mater.* **2017, 4**, 025112.
(22) Rivera, P.; Seyler, K. L.; Yu, H.; Schaibley, J. R.; Yan, J.; Mandrus, D. G.; Yao, W.; Xu, X. Valley-Polarized Exciton Dynamics in a 2D Semiconductor Heterostructure. *Science.* **2016**, *351* (6274), 688–691.
(23) Rivera, P.; Yu, H.; Seyler, K. L.; Wilson, N. P.; Yao, W.; Xu, X. Interlayer Valley Excitons in Heterobilayers of Transition Metal Dichalcogenides. *Nat. Nanotechnol.* **2018**, *13* (11), 1004–1015.
(24) Wse, M.; Rivera, P.; Schaibley, J. R.; Jones, A. M.; Ross, J. S.; Wu, S.; Aivazian, G.; Klement, P.; Seyler, K.; Clark, G.; Ghimire, N. J.; Yan, J.; Mandrus, D. G.; Yao, W.; Xu, X. Observation of Long-Lived Interlayer Excitons in monolayer $MoSe_2$-$WSe_2$ heterostructures. **2015**, 6242.
(25) Schaibley, J. R.; Rivera, P.; Yu, H.; Seyler, K. L.; Yan, J.; Mandrus, D. G.; Taniguchi, T.; Watanabe, K.; Yao, W.; Xu, X. Directional Interlayer Spin-Valley Transfer in Two-Dimensional Heterostructures. *Nat. Commun.* **2016**, *7*, 13747.
(26) Yan, T.; Yang, S.; Li, D.; Cui, X. Long Valley Relaxation Time of Free Carriers in Monolayer $WSe_2$. *Phys. Rev. B* **2017**, *95*, 241406.
(27) McCormick, E. J.; Newburger, M. J.; Luo, Y. K.; McCreary, K. M.; Singh, S.; Martin, I. B.; Cichewicz, E. J.; Jonker, B. T.; Kawakami, R. K. Imaging Spin Dynamics in Monolayer $WS_2$ by Time-Resolved Kerr Rotation Microscopy. *2D Mater.* **2018**, *5* (1), 011010.
(28) Volmer, F.; Pissinger, S.; Ersfeld, M.; Kuhlen, S.; Stampfer, C.; Beschoten, B. Intervalley Dark Trion States with Spin Lifetimes of 150 ns in $WSe_2$. *Phys. Rev. B* **2017**, *95* (23), 235408.
(29) Ersfeld, M.; Volmer, F.; De Melo, P. M. M. C.; De Winter, R.; Heithoff, M.; Zanolli, Z.; Stampfer, C.; Verstraete, M. J.; Beschoten, B. Spin States Protected from Intrinsic Electron-Phonon Coupling Reaching 100 ns Lifetime at Room Temperature in $MoSe_2$. *Nano Lett.* **2019**, *19* (6), 4083–4090.
(30) Li, J.; Goryca, M.; Yumigeta, K.; Li, H.; Tongay, S.; Crooker, S. A. Valley Relaxation of Resident Electrons and Holes in a Monolayer Semiconductor: Dependence on Carrier Density and the Role of Substrate-Induced Disorder. *Phys. Rev. Materials* **2021**, *5*, 044001.
(31) Zhu, H.; Wang, J.; Gong, Z.; Kim, Y. D.; Hone, J.; Zhu, X. Y. Interfacial Charge Transfer Circumventing Momentum Mismatch at Two-Dimensional van Der Waals Heterojunctions. *Nano Lett.* **2017**, *17* (6), 3591–3598.
(32) Ma, E. Y.; Guzelturk, B.; Li, G.; Cao, L.; Shen, Z. X.; Lindenberg, A. M.; Heinz, T. F. Recording Interfacial Currents on the Subnanometer Length and Femtosecond Time Scale by Terahertz Emission. *Sci. Adv.* **2019**, *5* (2), eaau0073.
(33) Komider, K.; González, J. W.; Fernández-Rossier, J. Large Spin Splitting in the

Conduction Band of Transition Metal Dichalcogenide Monolayers. *Phys. Rev. B - Condens. Matter Mater. Phys.* **2013**, *88* (24), 245436.
(34) Goryca, M.; Li, J.; Stier, A. V.; Taniguchi, T.; Watanabe, K.; Courtade, E.; Shree, S.; Robert, C.; Urbaszek, B.; Marie, X.; Crooker, S. A. Revealing Exciton Masses and Dielectric Properties of Monolayer Semiconductors with High Magnetic Fields. *Nat. Commun.* **2019**, *10* (1), 4172.
(35) Kang, J.; Tongay, S.; Zhou, J.; Li, J.; Wu, J. Band Offsets and Heterostructures of Two-Dimensional Semiconductors. *Appl. Phys. Lett.* **2013**, *102* (1), 012111.
(36) Ross, J. S.; Wu, S.; Yu, H.; Ghimire, N. J.; Jones, A. M.; Aivazian, G.; Yan, J.; Mandrus, D. G.; Xiao, D.; Yao, W.; Xu, X. Electrical Control of Neutral and Charged Excitons in a Monolayer Semiconductor. *Nat. Commun.* **2013**, *4*, 1474.
(37) Mak, K. F.; He, K.; Lee, C.; Lee, G. H.; Hone, J.; Heinz, T. F.; Shan, J. Tightly Bound Trions in Monolayer $MoS_2$. *Nat. Mater.* **2013**, *12* (3), 207–211.
(38) Klots, A. R.; Weintrub, B.; Prasai, D.; Kidd, D.; Varga, K.; Velizhanin, K. A.; Bolotin, K. I. Controlled Dynamic Screening of Excitonic Complexes in 2D Semiconductors. *Sci. Rep.* **2018**, *8*, 768.
(39) Wang, F.; Wang, J.; Guo, S.; Zhang, J.; Hu, Z.; Chu, J. Tuning Coupling Behavior of Stacked Heterostructures Based On $MoS_2$, $WS_2$, and $WSe_2$. *Sci. Rep*. ***2017***, 7, 44712.
(40) Greben, K.; Arora, S.; Harats, M. G.; Bolotin, K. I. Intrinsic and Extrinsic Defect-Related Excitons in TMDCs. *Nano Lett.* **2020**, *20* (4), 2544–2550.
(41) Kim, J.; Jin, C.; Chen, B.; Cai, H.; Zhao, T.; Lee, P.; Kahn, S.; Watanabe, K.; Taniguchi, T.; Tongay, S.; Crommie, M. F.; Wang, F. Observation of Ultralong Valley Lifetime in $WSe_2/MoS_2$ Heterostructures. *Sci. Adv.* **2017**, *3* (7), e1700518.
(42) Chen, H.; Wen, X.; Zhang, J.; Wu, T.; Gong, Y.; Zhang, X.; Yuan, J.; Yi, C.; Lou, J.; Ajayan, P. M.; Zhuang, W.; Zhang, G.; Zheng, J. Ultrafast Formation of Interlayer Hot Excitons in Atomically Thin $MoS_2/WS_2$ Heterostructures. *Nat. Commun.* **2016**, *7*, 12512.
(43) Plechinger, G.; Nagler, P.; Arora, A.; Schmidt, R.; Chernikov, A.; Del Águila, A. G.; Christianen, P. C. M.; Bratschitsch, R.; Schüller, C.; Korn, T. Trion Fine Structure and Coupled Spin-Valley Dynamics in Monolayer Tungsten Disulfide. *Nat. Commun.* **2016**, *7*, 12715.
(44) Dery, H.; Song, Y. Polarization Analysis of Excitons in Monolayer and Bilayer Transition-Metal Dichalcogenides. *Phys. Rev. B - Condens. Matter Mater. Phys.* **2015**, *92* (12), 125431.
(45) Yan T, Yu H, Xiao K, Yao W, Cui X. Probing the exciton k-space dynamics in monolayer tungsten diselenides. *2D Mater.* **2019**, 6(2), 025035.
(46) Kozawa, D.; Carvalho, A.; Verzhbitskiy, I.; Giustiniano, F.; Miyauchi, Y.; Mouri, S.; Castro Neto, A. H.; Matsuda, K.; Eda, G. Evidence for Fast Interlayer Energy Transfer in $MoSe_2/WS_2$ Heterostructures. *Nano Lett.* **2016**, *16* (7), 4087–4093.
(47) Kumar, N.; Cui, Q.; Ceballos, F.; He, D.; Wang, Y.; Zhao, H. Exciton-Exciton Annihilation in $MoSe_2$ Monolayers. *Phys. Rev. B - Condens. Matter Mater. Phys.* **2014**, *89* (12), 125427.
(48) Yu, Y.; Yu, Y.; Xu, C.; Barrette, A.; Gundogdu, K.; Cao, L. Fundamental Limits of Exciton-Exciton Annihilation for Light Emission in Transition Metal Dichalcogenide Monolayers. *Phys. Rev. B* **2016**, *93* (20), 201111.
(49) Harats, M. G.; Kirchhof, J. N.; Qiao, M.; Greben, K.; Bolotin, K. I. Dynamics and Efficient Conversion of Excitons to Trions in Non-Uniformly Strained Monolayer $WS_2$. *Nat. Photonics* **2020**, *14* (5), 324–329.

(50) Yuan, L.; Zheng, B.; Kunstmann, J.; Brumme, T.; Kuc, A. B.; Ma, C.; Deng, S.; Blach, D.; Pan, A.; Huang, L. Twist-Angle-Dependent Interlayer Exciton Diffusion in WS2–WSe2 Heterobilayers. *Nat. Mater.* **2020**, *19* (6), 617–623. https://doi.org/10.1038/s41563-020-0670-3.

(51) Altmann, P.; Sangalli, D.; Wang, Z.; Molina-sa, A.; Fazio, D. De; Soavi, G.; Sassi, U.; Bottegoni, F.; Ciccacci, F.; Finazzi, M.; Wirtz, L.; Ferrari, A. C.; Marini, A.; Cerullo, G.; Conte, S. D. Intravalley Spin − Flip Relaxation Dynamics in Single-Layer $WS_2$. Nano Lett. **2018***, 18*, 6882-6891.

(52) Zeng, H.; Dai, J.; Yao, W.; Xiao, D.; Cui, X. Valley Polarization in $MoS_2$ Monolayers by Optical Pumping. *Nat. Nanotechnol.* **2012**, *7* (8), 490–493.

(53) Carvalho, B. R.; Wang, Y.; Mignuzzi, S.; Roy, D.; Terrones, M.; Fantini, C.; Crespi, V. H.; Malard, L. M.; Pimenta, M. A. Intervalley Scattering by Acoustic Phonons in Two-Dimensional $MoS_2$ Revealed by Double-Resonance Raman Spectroscopy. *Nat. Commun.* **2017**, *8*, 14670.

(54) Kioseoglou, G.; Hanbicki, A. T.; Currie, M.; Friedman, A. L.; Jonker, B. T. Optical Polarization and Intervalley Scattering in Single Layers of $MoS_2$ and $MoSe_2$. *Sci. Rep.* **2016**, *6*, 25041.

(55) Plechinger, G.; Nagler, P.; Schüller, C.; Korn, T. Time-Resolved Kerr Rotation Spectroscopy of Valley Dynamics in Single-Layer $MoS_2$. arXiv:1404.7674, ver. 3, [cond-mat.mes-hall] **2014**; e-print archive, http://arxiv.org/abs/1404.7674v3 (accessed 2021-03-10).

(56) Jin, C.; Kim, J.; Iqbal Bakti Utama, M.; Regan, E. C.; Kleemann, H.; Cai, H.; Shen, Y.; Shinner, M. J.; Sengupta, A.; Watanabe, K.; Taniguchi, T.; Tongay, S.; Zettl, A.; Wang, F. Imaging of Pure Spin-Valley Diffusion Current in $WS_2$-$WSe_2$ Heterostructures. *Science.* **2018**, *360* (6391), 893–896.